Galaxy Dynamics: from the Early Universe to the Present
ASP Conference Series, Vol. in press, 1999
F. Combes, G. A. Mamon and V. Charmandaris, eds.

Orbital structure and dark haloes of elliptical galaxies

Andi Kronawitter (1), Ortwin E. Gerhard (1),
R. P. Saglia (2), Ralf Bender (2)

(1) Astronomisches Institut Universität Basel,
(2) Universitätssternwarte München

1. Introduction

To constrain the formation of elliptical galaxies, it is vital to know their mass distribution and orbital structure. Are the haloes of ellipticals and spiral galaxies similar, for the same stellar mass? Do ellipticals also have flat rotation curves? What is the shape of the velocity ellipsoids? How do the models compare to the results of (N-body) simulations?

To find answers to some of these questions we have analysed a sample of 10 elliptical galaxies of type E0-1 with kinematic data out to between 0.8 to 2.6 R_e. Half of the galaxies in our sample appear to reach nearly flat rotation curves between 1-2R_e. 3/10 galaxies can be fitted well by a constant mass-to-light ratio (M/L) model but 7/10 require additional mass in the modelled range. All but one of the analysed galaxies are radially anisotropic at 0.5 R_e, with anisotropy possibly decreasing again towards larger radii.

2. Data and modelling

Here we present results for 10 ellipticals with kinematic data from our measurements (Gerhard *et al.* 1998, Saglia *et al.* 2000, Kronawitter *et al.* 2000) for eight galaxies, Rix *et al.* (1997) for NGC 2434, and Statler and Smecker-Hane (1999) for NGC 3379. Surface-brightness (SB) data are taken from the literature except for NGC 5846 where we have new photometry. Where available HST-profiles were supplemented at small radii.

The modelling technique follows the lines described in Gerhard *et al.* (1998) and Saglia *et al.* (2000): first, we determine the density profile and the potential for the luminous matter from the smoothed SB-profile, assuming spherical symmetry. Then we compute 59 basis functions for the phase-space distribution (DF), each reproducing the stellar density, in a series of potentials including nonsingular isothermal dark matter halos with various core radii and circular speeds. We project these into the space of kinematic observables, and then fit to the measured σ and h_4 by a regularised least-squares algorithm, imposing non-negativity and smoothness of the composite DF. In this way, we find the unique best DF for every potential, and by varying the dark matter component of the potential we determine the range of potentials consistent with the data.

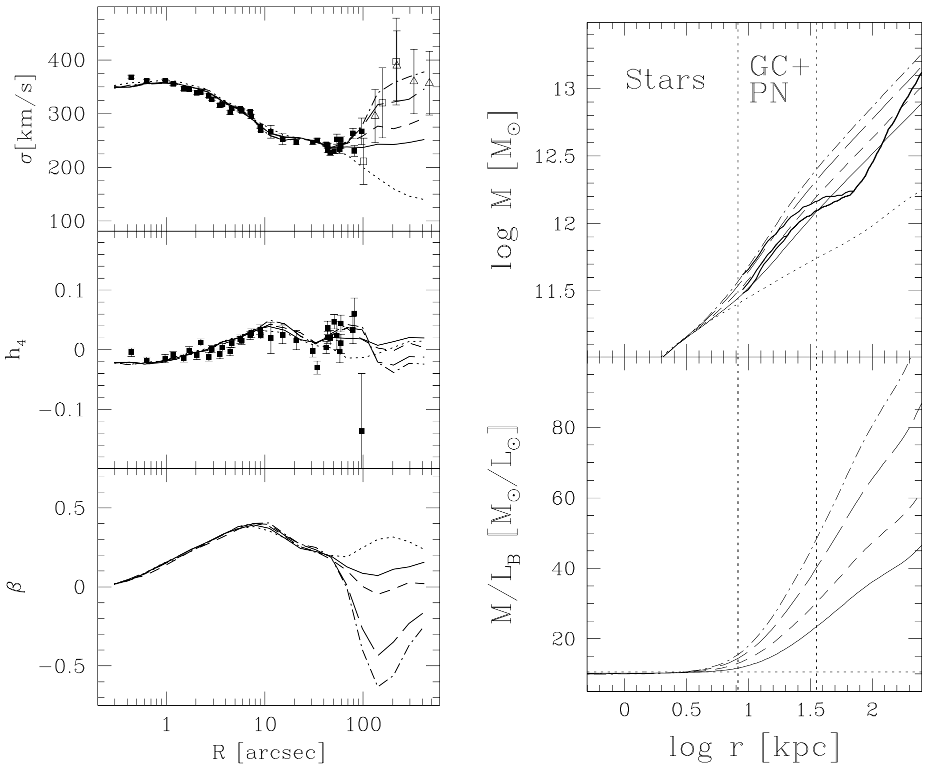

Figure 1. Left panel: Kinematic data and model fits for NGC 1399. From top to bottom, panels show the velocity dispersion σ, line profile parameter h_4, and intrinisic velocity anisotropy $\beta = 1 - \sigma_t^2/\sigma_r^2$. Besides the absorption line data we show velocity dispersions for 37 planetary nebulae from Arnaboldi *et al.* (1993, squares) and for 74 globular clusters from Kissler-Patig *et al.* (1998, triangles). The dotted line shows the constant mass-to-light ratio model; the other four lines correspond to halo models with increasingly massive halos. Right panel: Comparison of the mass profiles derived from X-ray data (Ikebe *et al.* 1996, thick lines) with our models (linestyles as in left panel). The X-ray mass profiles split due to uncertainties in the modelling of the temperature gradient. The vertical lines indicate the range of the absorption line data and the GC/PN data, respectively.

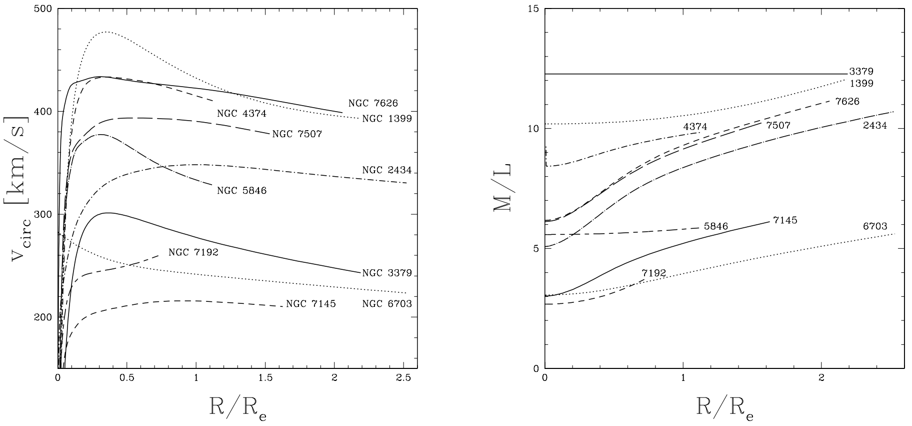

Figure 2. Left panel: Circular velocity curves from best-fit models for our sample of elliptical galaxies. Radius is given in units of the effective radius. Right panel: Corresponding cumulative mass-to-light ratio in the R-band (NGC 3379, NGC 7192), V-band (NGC 2434, NGC 5846 and NGC 7145) and B-band (all others), versus radius. All galaxies with extended data but NGC 3379 have M/L profiles rising outwards.

3. Results

Figure 1 shows the resulting model fits for NGC1399. The constant M/L model is not a good fit to the data, but this only becomes clear from the data points outside $R \simeq 50$ arcsec, especially with the planetary nebulae (PN) and globular cluster (GC) points. Both these tracers show an increase in the velocity dispersion from 250 km/s to 350 km/s outside 100 arcsec. Since both samples may be contaminated by intracluster objects, we have excluded the 10 % and 20 % fastest velocities, respectively, to test the robustness of our results. This does not change the preferred range of potentials for the GCs whereas the PN dispersions are quite sensitive and would then favour considerably less massive halos.

Figure 2 shows the circular velocity curves and mass-to-light ratios derived from our best-fit models for the entire sample. From χ^2-v_c-diagrams for the respective full set of models, we conclude that five of the ten objects reach a nearly flat rotation curve between 1-2R_e (NGC 2434, 6703, 7145, 7507, 7626). Two others require dark matter in the outer part of the modelled radial range (NGC 1399, 7192), and the remaining three (NGC 3379, 4374, 5846) are consistent within the errors with a constant mass-to-light ratio model. In NGC 3379, the constant M/L model provides the best fit to the data; this is also confirmed by the 29 PN velocities at larger radii (Ciardullo et al. 1993). The large mass-to-light ratio in NGC 3379 could in fact indicate the presence of dark matter, with a distribution that follows closely that of the luminous matter.

All but one galaxy show radial anisotropy of the velocity distribution at 0.5 R_e (Fig. 3). The exception is NGC 7626 which is classified as E pec. In the outer parts, where however the kinematical data are sparse and have large errors, the best-fit models become more isotropic or perhaps even tangentially

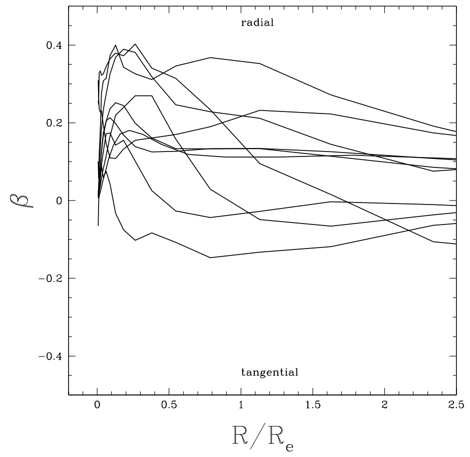

Figure 3. Intrinsic velocity anisotropy profiles derived from best-fit models for all sample galaxies. All but one galaxy (NGC 7626) show radial anisotropy at 0.5 R_e. The outer decline is often not well established since it depends on the outer data points which have relatively large errors; for a good case, see NGC 1399 in Fig. 1.

anisotropic. In most cases the outer decrease of β is not a firm result, since it depends sensitively on the outer data points; for a good case, see NGC 1399 in Fig. 1.

Since we modelled these galaxies under the assumption of spherical symmetry, one might argue that the shape of the anisotropy profiles could be altered if the galaxies were in reality flattened or elongated along the line of sight. However, several models of flattened giant ellipticals (e.g., NGC 1600, Matthias and Gerhard, 1999) have very similar radial anisotropy profiles. These oblate-axisymmetric three-integral models are fitted to both major and minor axis kinematic data.

References

Arnaboldi, M., Freeman, K.C., Hui, X., Capaccioli, M., Ford, H., 1994, The Messenger 76, 40

Ciardullo, R.,Jacoby, G.H., Dejonghe, H.B., 1993, ApJ, 414, 454

Gerhard, O. E., Jeske, G., Saglia, R. P., Bender, R. 1998, MNRAS, 295, 197

Ikebe, Y. *et al.* , 1996, Nature, 379, 427

Kissler-Patig, M., Brodie, J.P., Schroder, L.L., Forbes, D. A., Grillmair, C.J., Huchra, J.P., 1998, ApJ, 115, 105

Kronawitter, A., Saglia, R.P., Gerhard, O. E., Bender, R., 2000, in prep.

Matthias, M., Gerhard, O.E., 1999, MNRAS, in press

Rix, H.-W., de Zeeuw, P. T., Cretton, N., van der Marel, R., Carollo, M. C. 1997, ApJ, 488, 702

Saglia, R.P., Kronawitter, A., Gerhard, O.E., Bender, R. 2000, AJ, in press

Statler, T.S., Smecker-Hane, T., 1999, AJ, 117, 839